

Copyright © 1995, by the author(s).
All rights reserved.

Permission to make digital or hard copies of all or part of this work for personal or classroom use is granted without fee provided that copies are not made or distributed for profit or commercial advantage and that copies bear this notice and the full citation on the first page. To copy otherwise, to republish, to post on servers or to redistribute to lists, requires prior specific permission.

**REVIEW OF ION ENERGY DISTRIBUTIONS
IN CAPACITIVELY COUPLED RF PLASMA
REACTORS**

by

**E. Kawamura, V. Vahedi, M. A. Lieberman, and
C. K. Birdsall**

Memorandum No. UCB/ERL M95/49

15 June 1995

**REVIEW OF ION ENERGY DISTRIBUTIONS
IN CAPACITIVELY COUPLED RF PLASMA
REACTORS**

by

**E. Kawamura, V. Vahedi, M. A. Lieberman, and
C. K. Birdsall**

Memorandum No. UCB/ERL M95/49

15 June 1995

ELECTRONICS RESEARCH LABORATORY

**College of Engineering
University of California, Berkeley
94720**

Review of Ion Energy Distributions in Capacitively Coupled RF Plasma Reactors

E. Kawamura[†], V. Vahedi*, M. A. Lieberman[†], and C. K. Birdsall[†]

[†] Department of Electrical Engineering and Computer Science
University of California, Berkeley
Berkeley, CA 94720

* Lawrence Livermore National Laboratory, Livermore, CA 94550

We present a historical review and discussion of previous works on ion energy distributions (IED) arriving at the target in the collisionless sheath regime of a capacitively coupled rf discharge (RIE system). This regime is of great interest to experimentalists and modelers studying the new generation of high density discharges in which the sheath is much thinner than in the conventional RIE systems. The purpose of the review is to assess what has been done so far, to determine what factors influence the shape of the IEDs, and to clarify some issues about sheaths in high density systems. Having determined the important parameters, we perform some particle-in-cell simulations for a capacitively coupled rf plasma, which show that ion modulations in an rf sheath significantly affect the IEDs when $\tau_{ion}/\tau_{rf} < 1$, where τ_{ion} is the ion transit-time and τ_{rf} is the rf period.

I. Introduction

In processing plasmas, the ion energy and angular distributions (IED and IAD) arriving at the target are crucial in determining anisotropy and etch rates. Gottscho *et al*¹ (1992) presented an excellent review and description of microscopic uniformity in plasma etching. They show that whenever the etching rate depends on the ion energy flux, the ion angular distribution will influence the etching profile and will contribute towards the aspect ratio dependence of the etching rate. For example, in collisional sheaths, ions undergoing collisions as they are accelerated across the sheath will arrive at the wafer surface with hyperthermal energies and off-normal angles of incidence. If the ion energies are in excess of the reactive sputter threshold, ion enhanced etching will occur on the sidewalls as well as on the bottom surface. Under these conditions, the number of ions able to impact the bottom surface relative to the number impacting the sidewalls will decrease as the aspect ratio increases. This scenario qualitatively accounts for RIE lag and such profile phenomena as sidewall bowing.²

Zarowin³(1984) pointed out the importance of off-normal ion incidence in determining reactively ion etched profiles. He discussed how the IED can induce anisotropic etch reactions, and under certain circumstances can “enhance” the intrinsic chemical etch selectivity. However, Zarowin’s analysis of the ion transport assumes that the perpendicular ion temperature, which determines the off-normal flux, remains invariant as ions cross the sheath and undergo ion-neutral collisions. This assumption is valid for charge exchange collisions but not for elastic scattering.

Due to high operating pressures (\sim few hundred mtorr) and large sheath voltage drops (\sim 1000 V), the sheaths in conventional capacitively coupled plasma sources are typically collisional. Most of the ion energy spread is caused by ion-neutral collisions. In this regime, the IED was shown to have multiple peaks and a large spread.⁴⁻⁸ Davis and Vanderslice⁹ (1963) were among the first to present experimental measurements of IEDs in dc glow discharges. Their measurements were made at relatively high pressures where the sheaths were highly collisional and most ions arrived at the target at low energies. Davis and Vanderslice⁹ also

presented a simple model to describe IEDs in a dc collisional sheath, which compared well with their IEDs and which has been verified by other experiments and simulations (Vahedi *et al*¹⁰ 1991).

A new generation of high density plasma sources is now being widely studied and characterized due to their potential use in semiconductor manufacturing and fabrication.¹¹⁻¹⁴ These plasma sources are typically operated at higher densities and lower pressures in order to obtain higher etch rates and better ion anisotropy at the target. Furthermore, most of the new high density sources operate with reduced sheath voltage drops in order to reduce ion bombarding damage and achieve ion energy control. In this regime, the ion motion in the rf sheath is essentially collisionless since the sheath width is much smaller than the ion mean free path. Ion energy and angular spreads due to collisions within the sheaths are minimal. In this paper, we review and discuss ion modulation within a collisionless sheath, which can cause large ion energy spreads and can also give rise to angular spreads.

II. Review of Ion Sheath Modulation

Because of the complexity of rf sheath dynamics, most calculations of IEDs rely on numerical methods. Closed form analytical expressions for IEDs in rf plasma reactors are rare and obtainable only after making very limiting approximations. IEDs have been calculated by approximate analytical models,¹⁵⁻¹⁷ the numerical integration of the equations of motion,^{18,19,4,5,7,20} Monte-Carlo simulations,^{21,22,6,23,24} a Monte-Carlo-fluid hybrid model,²⁵ a particle-in-cell (PIC) method,²⁶ and a particle-in-cell method combined with Monte-Carlo collisions (PIC-MCC).²⁷ Many of the methods use presupposed fields and initial ion velocity distributions, while others try to obtain these self-consistently.

The energies of the bombarding ions have been measured by electrostatic deflection analysers,^{28-32,13,33} cylindrical mirror analysers³⁴⁻⁴⁰ or retarding grid analysers.^{4-6,11,14,41} The energies were measured at the grounded electrode or at the powered electrode of the rf reactor. In some cases, quadrupole mass spectrometers were used to make mass resolved measurements. This has made it possible to compare the IEDs of different ionic species in

the same sheath.

A. Ratio of ion transit time to rf period: τ_{ion}/τ_{rf}

In collisionless sheaths, the crucial parameter determining the shape of the IEDs is $\tau_{ion}/\tau_{rf} = \omega_{rf}/\omega_{ion}$, where $\tau_{rf} = 2\pi/\omega_{rf}$ is the rf period and $\tau_{ion} = 2\pi/\omega_{ion}$ is the time an ion takes to traverse the sheath when the sheath drop is at its dc value \bar{V}_s . If we assume a collisionless Child-Langmuir space charge sheath, then the spatial variation of the sheath potential is given by $V_s(x) = C_1 x^{4/3}$, where $C_1 = (9J_i/(4\epsilon_0))^{2/3}(M/(2e))^{1/3}$ is independent of x . Here, J_i is the ion conduction current, and M is the ion mass. Also, if we neglect the initial ion velocity, then the ion velocity is given by $v(x) = (2eV_s(x)/M)^{1/2}$. Then,

$$\tau_{ion} = \int_0^{\bar{s}} \frac{dx}{v(x)} = \left(\frac{M}{2eC_1}\right)^{1/2} \int_0^{\bar{s}} x^{-2/3} dx = \left(\frac{M}{2eC_1}\right)^{1/2} 3\bar{s}^{1/3} = 3\bar{s} \left(\frac{M}{2e\bar{V}_s}\right)^{1/2}, \quad (1)$$

where \bar{s} is the time-averaged sheath thickness. So, the ratio of τ_{ion} with respect to the rf period τ_{rf} is just

$$\frac{\tau_{ion}}{\tau_{rf}} = \frac{3\bar{s}\omega_{rf}}{2\pi} \left(\frac{M}{2e\bar{V}_s}\right)^{1/2}. \quad (2)$$

For $\tau_{ion}/\tau_{rf} \ll 1$, the ions cross the sheath in a small fraction of an rf cycle and respond to the instantaneous sheath voltage. Thus, their final energies depend strongly on the phase of the rf cycle in which they enter the sheath. As a result, the IED is broad and bimodal, and the IED width ΔE_i approaches the peak to peak sheath voltage. The two peaks in the distribution correspond to the minimum and maximum sheath drops (i.e., where the voltage is most slowly varying). For $\tau_{ion}/\tau_{rf} \gg 1$, the ions take many rf cycles to cross the sheath and can no longer respond to the instantaneous sheath voltage. Instead, the ions respond only to an average sheath voltage, and the phase of the cycle in which they enter the sheath becomes unimportant, resulting in a narrower energy distribution. In this high frequency regime, ΔE_i was calculated analytically for a collisionless sheath by Benoit-Cattin *et al*¹⁵(1967) and found to be directly proportional to τ_{rf}/τ_{ion} . Thus, as τ_{ion}/τ_{rf} increases, the IED width shrinks and the two peaks of the IED approach each other until, at some point, they can no longer be resolved.

One of the earliest works to show ion sheath modulation is the laboratory measurements of Erö²⁸ (1958). He experimentally measured the IED in a Thoneman ion source and observed the effect of rf modulation on IED width ΔE_i . His ion energy spectra had the characteristic bimodal shape, shown schematically in Figure 1. He observed that as the applied rf voltage was raised, ΔE_i increased.

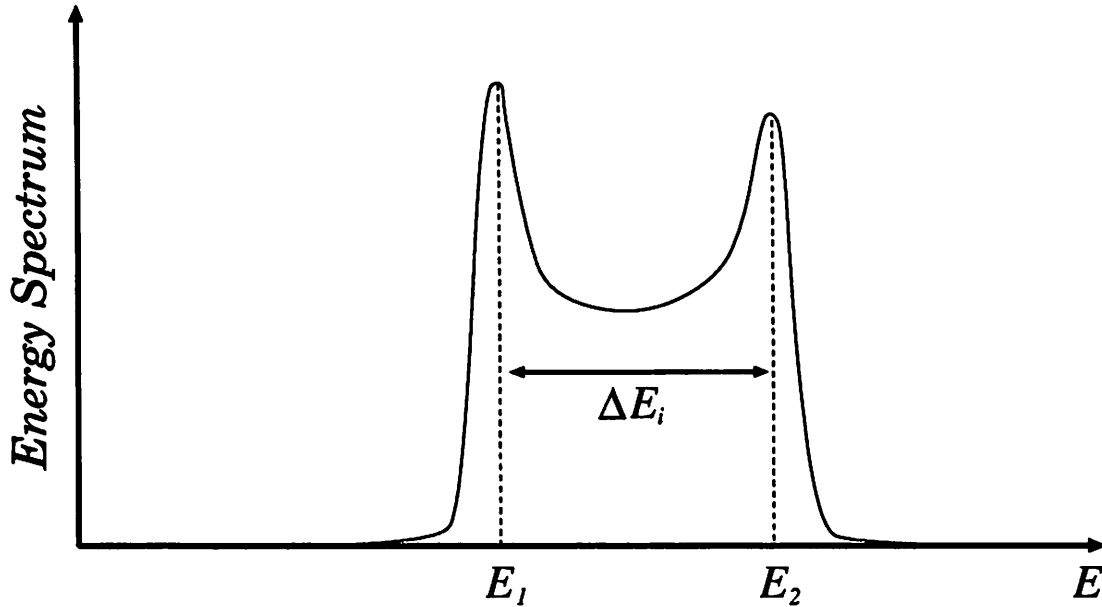


Figure 1:

B. Analytic Calculation of IED and ΔE_i for $\tau_{ion}/\tau_{rf} \gg 1$

Benoit-Cattin *et al*¹⁵ (1967) analytically calculated the IED and ΔE_i in the high frequency regime ($\tau_{ion}/\tau_{rf} \gg 1$) for a collisionless rf sheath. They assumed (i) a constant sheath width, (ii) a uniform sheath electric field, (iii) a sinusoidal sheath voltage $V_s(t) = \bar{V}_s + \tilde{V}_s \sin \omega_{rf} t$, and (iv) zero initial ion velocity at the plasma-sheath boundary. The resulting expressions for ΔE_i and the IED are

$$\Delta E_i = \frac{2e\tilde{V}_s}{\bar{s}\omega_{rf}} \left(\frac{2e\bar{V}_s}{M} \right)^{1/2} = \frac{3e\tilde{V}_s}{\pi} \left(\frac{\tau_{rf}}{\tau_{ion}} \right), \quad (3)$$

and

$$f(E) = \frac{dn}{dE} = \frac{2n_0}{\omega_{rf}\Delta E_i} \left[1 - \frac{4}{\Delta E_i^2} (E - e\bar{V}_s)^2 \right]^{-1/2}, \quad (4)$$

where n_0 is the number of ions entering the sheath per unit time. The calculations yield a bimodal IED with two peaks symmetric about $e\bar{V}_s$, and ΔE_i proportional to τ_{rf}/τ_{ion} . As ω_{rf} or ion mass M is increased, ΔE_i is reduced and the two peaks of the IED approach each other. The two peaks of the calculated IED are singular because of the assumed monoenergetic initial velocity distribution.

It is instructive to derive equations (3) and (4). We begin with the equation of motion under the assumption of a uniform sheath field and a sinusoidal sheath voltage.

$$M \frac{dv}{dt} = \frac{e}{s} (\bar{V}_s + \tilde{V}_s \sin \omega_{rf} t). \quad (5)$$

Let t_0 be the time the ion enters the sheath. And let t_1 be the time the ion hits the target. Then, integrating the equation of motion once and assuming $v(t_0) = 0$, we obtain

$$Mv(t_1) = \frac{e\bar{V}_s}{s} (t_1 - t_0) + \frac{e\tilde{V}_s}{\omega_{rf}s} (\cos \omega_{rf} t_1 - \cos \omega_{rf} t_0). \quad (6)$$

Let us define the dimensionless parameter

$$A \equiv \frac{\omega_{rf}^2 s^2 M}{e\bar{V}_s}. \quad (7)$$

From equation (1), we see that $A = 8\pi^2/9(\tau_{ion}/\tau_{rf})^2$. Using $E = Mv(t_1)^2/2$, and rearranging equation (6), we get an expression for the normalized energy,

$$\frac{E}{e\bar{V}_s} = \frac{1}{2A} \left[\omega_{rf}(t_1 - t_0) - \frac{\tilde{V}_s}{\bar{V}_s} (\cos \omega_{rf} t_1 - \cos \omega_{rf} t_0) \right]^2. \quad (8)$$

If we now integrate equation (6), we get

$$s = x(t_1) - x(t_0) = \frac{e\bar{V}_s M (t_1 - t_0)^2}{2s} + \frac{e\tilde{V}_s M (t_1 - t_0) \cos \omega_{rf} t_0}{\omega_{rf} s} - \frac{e\tilde{V}_s M (\sin \omega_{rf} t_1 - \sin \omega_{rf} t_0)}{s\omega_{rf}^2}. \quad (9)$$

Rearranging terms, we get an expression for A ,

$$A \equiv \frac{s^2 M \omega_{rf}^2}{e\bar{V}_s} = \frac{\omega_{rf}^2 (t_1 - t_0)^2}{2} + \frac{\tilde{V}_s}{\bar{V}_s} [\omega_{rf} (t_1 - t_0) \cos \omega_{rf} t_0 - (\sin \omega_{rf} t_1 - \sin \omega_{rf} t_0)]. \quad (10)$$

Now, if we assume the high frequency case, then the ion transit time across the sheath is much larger than the rf period. This implies that $\omega_{rf}(t_1 - t_0) \gg 1$. It also implies that $A \sim (\tau_{ion}/\tau_{rf})^2 \gg 1$. So, if we look at expression (8) for the normalized energy and expression (10) for A , we note that the terms proportional to $\omega_{rf}(t_1 - t_0)$ or $\omega_{rf}^2(t_1 - t_0)^2$ are much larger than the other terms which are roughly of order unity. Thus, we can write

$$\frac{E}{e\bar{V}_s} \approx \frac{1}{A} \left[\frac{\omega_{rf}^2(t_1 - t_0)^2}{2} - \frac{\tilde{V}_s}{V_s} \omega_{rf}(t_1 - t_0) (\cos \omega_{rf} t_1 - \cos \omega_{rf} t_0) \right]. \quad (11)$$

and

$$A \approx \frac{\omega_{rf}^2(t_1 - t_0)^2}{2} + \frac{\tilde{V}_s}{V_s} \omega_{rf}(t_1 - t_0) \cos \omega_{rf} t_0. \quad (12)$$

Then, we find

$$\frac{E}{e\bar{V}_s} \approx \frac{1}{A} \left[A - \frac{\tilde{V}_s}{V_s} \omega_{rf}(t_1 - t_0) \cos \omega_{rf} t_1 \right] = 1 - \frac{\tilde{V}_s}{V_s A} \omega_{rf}(t_1 - t_0) \cos \omega_{rf} t_1. \quad (13)$$

Also, solving for $\omega_{rf}(t_1 - t_0)$ in the expression for A , we get

$$\omega_{rf}(t_1 - t_0) = \sqrt{2A} + \Theta(1). \quad (14)$$

Note that because $A \gg 1$, the $\Theta(1)$ expression may be neglected. Substituting this into the expression for normalized energy, we get

$$\frac{E}{e\bar{V}_s} \approx 1 - \sqrt{\frac{2}{A}} \frac{\tilde{V}_s}{V_s} \cos \omega_{rf} t_1. \quad (15)$$

This implies that the normalized energy spread is

$$\frac{\Delta E_i}{e\bar{V}_s} = 2\sqrt{\frac{2}{A}} \frac{\tilde{V}_s}{V_s} = \frac{2\tilde{V}_s}{V_s \omega_{rf} s} \left(\frac{2e\bar{V}_s}{M} \right)^{1/2}. \quad (16)$$

This is equivalent to Benoit-Cattin *et al*'s expression for ΔE_i (equation 3). To get the ion energy distribution, we note that

$$f(E) = \frac{dn}{dE} = \frac{dn}{dt_0} \frac{dt_0}{dE}. \quad (17)$$

If we assume constant ion flux, then $dn/dt_0 = n_0$ is a constant. Also, from the above, we have

$$E - e\bar{V}_s \approx \frac{\Delta E_i}{2} \cos(\omega_{rf} t_0 + \sqrt{A}). \quad (18)$$

This implies that

$$\frac{dE}{dt_0} \approx \frac{\Delta E_i}{2} \omega_{rf} \sin(\omega_{rf} t_0 + \sqrt{A}). \quad (19)$$

Substituting this into the expression for $f(E)$ and using the trigonometric identity $\sin \theta = \sqrt{1 - \cos^2 \theta}$, we obtain Benoit-Cattin *et al*'s expression

$$f(E) = \frac{dn}{dE} = \frac{2n_0}{\Delta E_i \omega_{rf}} \left[1 - \frac{4}{\Delta E_i^2} (E - e\bar{V}_s)^2 \right]^{-1/2}. \quad (20)$$

Benoit-Cattin *et al* also made the additional assumption that $\tilde{V}_s/\bar{V}_s \ll 1$. But from the above derivation, we see that this assumption is not necessary to derive equations (3) and (4), provided that we assume that the ion transit time is much larger than the rf period.

In a later paper, Benoit-Cattin and Bernard¹⁶ (1968) assumed a more realistic Child-Langmuir space charge sheath electric field rather than a uniform sheath electric field when computing IED and ΔE_i in a collisionless rf sheath. They still only considered the high frequency regime ($\tau_{ion}/\tau_{rf} \gg 1$) and assumed constant sheath width, sinusoidal sheath voltage, and null initial ion velocity at the plasma-sheath boundary. Except for numerical factors of order unity, their results were the same as in their previous paper. The revised ΔE_i is given by

$$\Delta E_i = \frac{8e\tilde{V}_s}{3\bar{s}\omega_{rf}} \left(\frac{2e\bar{V}_s}{M} \right)^{1/2} = \frac{4e\tilde{V}_s}{\pi} \left(\frac{\tau_{rf}}{\tau_{ion}} \right). \quad (21)$$

This suggests that while the ion modulation is very important, the exact profile of the electric field in the sheath does not change the overall ion modulation result significantly. Okamoto and Tamagawa²⁹ (1970) did a similar calculation and obtained the same ΔE_i as Benoit-Cattin and Bernard; they also experimentally verified the dependence of ΔE_i on frequency, ion mass and applied rf voltage.

C. Numerical Integration of Equations of Motion

Tsui¹⁸ (1968) numerically integrated the equations of motion in order to obtain IEDs in a collisionless rf sheath. He noted the dependence of IEDs on the parameter $a_i = (4e\bar{V}_s)/(M\omega_{rf}^2\bar{s}^2) \approx 0.5(\tau_{rf}/\tau_{ion})^2$. In his calculations, he assumed (*i*) a constant sheath

width, (ii) a spatially linearly-varying sheath electric field, (iii) a sinusoidal sheath voltage, (iv) $T_i = T_e$, where T_i and T_e are the bulk plasma ion and electron temperatures, and (v) a Maxwellian initial ion velocity distribution at the plasma-sheath boundary with $v_{th} = (kT_i/M)^{1/2}$. In general, $T_i \ll T_e$, so that assumption (iv) is invalid. But this did not affect the overall results since in Tsui's calculations, T_i is important only in determining the initial ion velocity distribution. For final velocity v_f much greater than the initial velocity v_o , (the usual case), the IEDs are insensitive to initial ion velocities. Tsui also saw bimodal IEDs centered about $e\bar{V}_s$. For higher a_i (lower τ_{ion}/τ_{rf}), the IEDs became wider and the low energy peak disappeared. For lower a_i (higher τ_{ion}/τ_{rf}), the two peaks became more equal in height and approached each other.

The disappearance of the low energy peak for small τ_{ion}/τ_{rf} in Tsui's IED diagrams is due to Tsui's assumption of constant sheath width. When $\tau_{ion}/\tau_{rf} \ll 1$, the ions traverse the sheath in a small fraction of an rf cycle. Hence, the high energy peak occurs when ions enter the sheath near a maximum sheath voltage, while the low energy peak occurs when ions enter the sheath near a minimum sheath voltage. If we take the sheath width oscillation into account, the low energy ions which enter the sheath near a minimum voltage see a shorter sheath width than the high energy ions which enter the sheath near a maximum voltage. Due to their shorter path, low energy ions can traverse the sheath without seeing a significant spread in the voltage. On the other hand, due to their greater acceleration, high energy ions can also cross the sheath without seeing a significant spread in the voltage. But if we neglect the sheath width oscillation and assume the sheath width is fixed, then the low energy ions must travel as long a path as the high energy ions. As a result, the low energy ions stay longer in the sheath and see a greater spread of voltages. Thus, at constant sheath width, the low energy peak disappears. This is why in Tsui's IEDs, the low energy peaks become smaller as τ_{ion}/τ_{rf} decreases. This implies that sheath width oscillation must be included in order to obtain realistic IEDs at small τ_{ion}/τ_{rf} . On the other hand, constant sheath width is not a bad assumption for the high frequency regime where $\tau_{ion}/\tau_{rf} \gg 1$.

D. Sheath Impedance, Resistive or Capacitive

Whether or not the high energy peak or low energy peak of the IED dominates at low τ_{ion}/τ_{rf} depends on whether or not the sheath voltage $V_s(t)$ is mostly at a maximum or minimum during an rf cycle. The sheath voltage waveform depends strongly on the nature of the sheath, i.e., whether it is resistive or capacitive. A sheath is resistive if $J_c \gg J_d$, and it is capacitive if $J_c \ll J_d$, where J_c is the conduction current density and J_d is the displacement current density. For a capacitive sheath driven by a sinusoidal voltage source, the sheath voltage is a symmetric sine wave. Therefore, within one cycle, the sheath drop is at a minimum for as long as it is at a maximum. As a result, the two peaks of the collisionless IED are more or less of equal height. For a resistive sheath, the sheath voltage is not a symmetric sine wave even when the sheath is driven by a sinusoidal voltage source. The target potential $V_T(t)$ is sinusoidal but the plasma potential $V_P(t)$ is highly non-sinusoidal, resulting in a non-sinusoidal sheath voltage $V_s(t) = V_P(t) - V_T(t)$. In fact, the sheath drop is at a minimum value longer than it is at a maximum value. As a result, the bimodal collisionless IEDs have dominant low energy peaks at low τ_{ion}/τ_{rf} . Hence as τ_{ion}/τ_{rf} increases, we see a transition from a resistive sheath with a broad bimodal IED and a dominant low energy peak to a capacitive sheath with a narrow bimodal IED and peaks of more or less equal height.

For a collisionless Child-Langmuir sheath, the ion conduction current is given by

$$J_i = \frac{4\epsilon_o}{9} \left(\frac{2e}{M} \right)^{1/2} \frac{\bar{V}_s^{3/2}}{\bar{s}^2}. \quad (22)$$

Let a displacement current be defined by,

$$J_d = \frac{\omega_{rf} \tilde{V}_s \epsilon_o}{\bar{s}}. \quad (23)$$

This implies that

$$\frac{J_i}{J_d} = \frac{2\tau_{rf}}{9\pi\bar{s}} \left(\frac{\bar{V}_s}{\tilde{V}_s} \right) \left(\frac{2e\bar{V}_s}{M} \right)^{1/2}. \quad (24)$$

Finally, by using $\tau_{ion} = 3\bar{s} \left(M/(2e\bar{V}_s) \right)^{1/2}$, we see that for a collisionless sheath,

$$\frac{J_i}{J_d} = \frac{2}{3\pi} \left(\frac{\bar{V}_s}{\tilde{V}_s} \right) \left(\frac{\tau_{rf}}{\tau_{ion}} \right). \quad (25)$$

Thus, if $\tau_{ion}/\tau_{rf} \ll 1$, the sheath tends to be resistive, whereas, if $\tau_{ion}/\tau_{rf} \gg 1$, the sheath tends to be capacitive.

E. Experiments

Coburn and Kay³⁰ (1972) presented experimental measurements of the rf modulation effect on IEDs and ΔE_i . Again, the IEDs depended on τ_{ion}/τ_{rf} . Coburn and Kay varied M rather than ω_{rf} , which they kept fixed at $\omega_{rf}/2\pi = 13.56$ MHz. They also saw the bimodal IEDs seen by Erö and calculated by Tsui and Benoit-Cattin *et al.* For larger values of τ_{ion}/τ_{rf} (i.e., larger M) the IEDs became narrower, as expected. In direct contrast to Tsui's results, the low energy peak of the IED tended to dominate at smaller values of τ_{ion}/τ_{rf} .

Kohler *et al.*³¹ (1985) presented a comprehensive set of experimental measurements of IEDs at the grounded surface of a low-pressure argon (50 mtorr) rf plasma reactor for frequencies of 70 kHz to 13.56 MHz. They discussed resistive sheaths (prevalent at low ω_{rf}) and capacitive sheaths (prevalent at high ω_{rf}), as well as direct coupling (dc-grounded excitation electrode) and capacitive coupling. They showed that the maximum ion energy depended strongly on the geometry of the system (asymmetric vs. symmetric), whether the excitation electrode was dc-grounded or capacitively coupled, and whether the sheaths were resistive or capacitive.

F. Simulations

Kushner²¹ (1985) used Monte-Carlo simulations to study the IED and the ion angular distribution (IAD) of ions in low-pressure capacitively coupled rf discharges, considering a parametric model for the sheath electric field: $E(x, t) = E_0[s(t) - x]^a$, $E_0 = V_s(t)(a + 1)/s(t)^{(a+1)}$. He also assumed a sinusoidally varying sheath width $s(t) = s_{dc} + s_{rf} \sin(\omega_{rf}t + \alpha)$. The ions were directed towards the sheath starting at a fixed location greater than the maximum sheath length with initial velocities randomly chosen from a Maxwellian distribution. Only charge exchange collisions were included in his model. Kushner also noted the dependence of the IED shapes on the parameter τ_{ion}/τ_{rf} .

Barnes *et al.*²³ (1991) used Monte-Carlo simulations to study ion kinetics in low pressure (~ 1 mtorr) rf glow discharge sheaths. Both charge exchange and elastic collisions were included in the model although collisions were not important at the very low pressures

they considered. They used various models for the sheath electric field (uniform, linear, Child-Langmuir and Lieberman⁴³). The ions were injected at the plasma-sheath boundary with an initial velocity randomly chosen from a Gaussian distribution. They also noted the importance of the parameter τ_{ion}/τ_{rf} in determining IED shapes.

G. Equivalent Circuit Model

Metze *et al*⁴² (1986) presented an equivalent circuit model for a planar rf plasma reactor. Their calculation was valid only in the low frequency regime ($\tau_{ion}/\tau_{rf} \ll 1$), where the ions are highly modulated and see the instantaneous sheath voltage drop. The model shows that the voltage drops across the sheaths are highly non-sinusoidal due to the non-linear properties of the sheath capacitances and the conduction currents. They saw that for a resistive sheath, the voltage drop across the sheath $V_s(t)$ is at a minimum value for a longer portion of the rf cycle than at a maximum value.

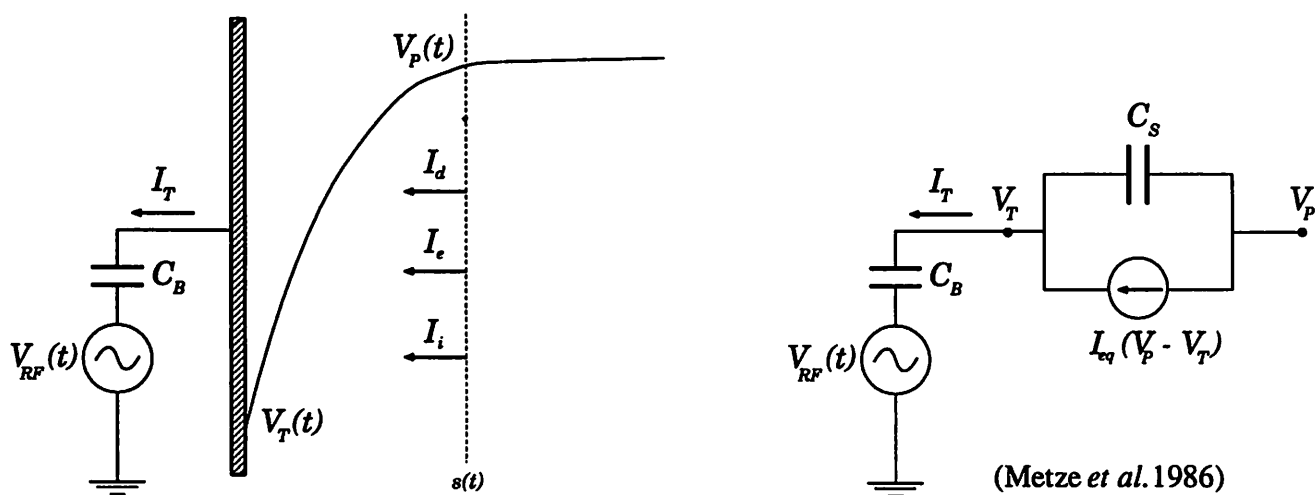


Figure 2:

Figure 2 illustrates the electron and ion conduction currents and the displacement current that flow through an rf sheath as well as an equivalent circuit model for the rf sheath proposed by Metze *et al.*⁴² The displacement current I_d can be modeled as the product of the time variation of the sheath voltage drop times a nonlinear capacitance defined for the rf sheath.

Assuming that the ions enter the sheath at the Bohm velocity $v_B = (kT_e/M)^{1/2}$ and that the electrons have a Boltzmann distribution in the sheath, one can write the total current flowing in the sheath as

$$\begin{aligned} I_T &= I_d + I_i + I_e, \\ &= C_s \frac{d}{dt}(V_P - V_T) + A_T n_s \left[v_B - \frac{\bar{v}_e}{4} \exp\left(\frac{-e(V_P - V_T)}{kT_e}\right) \right], \end{aligned} \quad (26)$$

where C_s is the sheath nonlinear capacitance, V_P is the instantaneous potential at the plasma-sheath boundary, V_T is the instantaneous potential at the wall (see Fig. 2), A_T is the electrode area, n_s is the density at the sheath edge, and T_e is the electron temperature. Metzger *et al.*¹² presented an expression for the nonlinear capacitance in the low frequency regime ($\tau_{ion}/\tau_{rf} \ll 1$) where the ions essentially respond to the instantaneous sheath voltage drop. By numerically solving the circuit equations, Metzger *et al.* determined the sheath voltage waveforms for $\tau_{ion}/\tau_{rf} \ll 1$.

In a related paper, Metzger *et al.*¹⁹ (1989) used the sheath voltage waveforms obtained from their equivalent circuit model to determine the IEDs for rf frequencies of 100 KHz and 13.56 MHz. Strictly speaking, their model was not valid at the higher frequency of 13.56 MHz. They saw bimodal IEDs in which the peak splitting decreases as frequency increases. They also observed that the IEDs were skewed toward low energies, especially at low τ_{ion}/τ_{rf} . This agrees well with the experimental results of Coburn and Kay as well as Kohler *et al.* For $\tau_{ion}/\tau_{rf} \ll 1$, the voltage across the sheath is at a minimum longer than it is at a maximum so that ions are accelerated by a small potential drop for a larger fraction of the rf cycle than for a large potential drop. This results in IEDs with dominant low energy peaks.

H. Idealized Analytical Model for $\tau_{ion}/\tau_{rf} \sim 1$

As τ_{ion}/τ_{rf} increases (i.e., high frequency case), we see that ΔE_i narrows systematically and the two peaks become more equal in height. But we often see an asymmetry in the peak heights even when the sheath is not resistive but approaches the capacitive case (i.e., $\tau_{ion}/\tau_{rf} > 1$ but not much greater than 1). Sometimes the asymmetry favors the high energy peak. Farouki *et al.*¹⁷ (1992) used an idealized analytical model to determine the relative

heights of the two peaks in a capacitive sheath. In their model they used a sinusoidally oscillating plasma-sheath boundary. Between the electrode and the plasma-sheath boundary, the electric field was uniform; outside this region, it was zero. The resulting IEDs were bimodal. Ions in the high energy peak generally had one less encounter with the oscillating plasma-sheath boundary than ions in the low energy peak. As the rf frequency was increased, they observed a systematic narrowing of the IEDs but the precise shapes of the IEDs exhibited rapid variations; they observed a “quasiperiodic” behavior in the relative prominence of the low and high energy peaks.

I. Collisional Effects and Ion Angular Distribution (IAD)

In collisionless sheaths, given the initial ion velocity distribution at the sheath edge, the ion angular distribution (IAD) can be deduced from the IED. However, this is not true for collisional sheaths. Collisional effects become important in conventional RIE reactors operated at high pressure. Both elastic and charge exchange collisions occur in the sheath and affect the IED and IAD. In elastic collisions, fast ions scatter against slow neutrals more or less isotropically. In charge exchange collisions, fast ions transfer their charge to slow neutrals, resulting in fast neutrals and slow ions. Both types of collisions broaden the IED and shift it towards lower energies. Charge exchange collisions also lead to the formation of secondary peaks in the IEDs at lower energies. The origin of these peaks was described by Wild and Koidl⁴ (1989). Recall that the two primary peaks are due to the rf modulation of slow ions which entered the sheath at the sheath edge and did not experience collisions. Similarly, the secondary peaks are due to the rf modulation of the slow ions resulting from charge exchange collisions within the sheath. These peaks are at lower energies, because the slow ions that are formed inside the sheath don't experience the full potential drop of the ions entering at the sheath edge. Elastic scattering can result in ions with appreciable transverse velocity and significantly broaden the IADs of ions hitting the target. Charge exchange collisions result in slow ions with no appreciable transverse velocity. Once the electric field accelerates these ions, most of their velocity will be parallel to the field. However, the IAD is still broadened from the collisionless case since charge exchange collisions decrease the

ratio of the parallel velocity component over the transverse velocity component. Because charge exchange collisions can produce fast neutrals that can bombard the target, it may be necessary to consider neutral energy and angular distributions when calculating sputter and etch yields in collisional sheaths.^{7,24}

J. Contradictions

In some of the numerical simulations of IEDs in collisionless sheaths at low frequencies (i.e., $\tau_{ion}/\tau_{rf} \ll 1$), we see cases where the low energy peak has vanished and the high energy peak is dominant. This is in direct contradiction to experimental results (i.e., Coburn and Kay³⁰ and Kohler³¹). The reason for this can be an assumption of constant sheath width as in Tsui's model. Or, it can be due to an incorrect choice of initial conditions. Many studies include the effects of oscillating sheath width in determining the sheath voltages, but neglect these effects when determining the starting positions of ions entering the sheath. They assume that all the ion trajectories start at a plane of origin $x = s_{max}$, the maximum sheath length despite the fact that the plasma-sheath boundary oscillates with time. This can have the same effect as assuming a constant sheath width. As described above, this will reduce the low energy peak when $\tau_{ion} \ll \tau_{rf}$. This is why, for collisionless rf reactors with $\tau_{ion} \ll \tau_{rf}$ (resistive sheath regime), we sometimes see low energy peaks of IEDs disappear in numerical simulations, but not in actual experiments.

K. Ion Plasma Frequency and Ion Transit Frequency

Some authors take the natural frequency of ions in the sheath to be the ion plasma frequency ω_{pi} rather than the ion transit frequency ω_{ion} . For typical parameters, ω_{pi} and ω_{ion} are close in value. The ion plasma frequency $\omega_{pi} = (ne^2/(\epsilon_o M))^{1/2}$, where n is the ion concentration in the bulk plasma, and the ion transit frequency $\omega_{ion} = 2\pi/\tau_{ion} = 2\pi(2e\bar{V}_s/M)^{1/2}/(3\bar{s})$. Then,

$$\frac{\omega_{pi}}{\omega_{ion}} = \frac{3\bar{s}}{2\pi} \left(\frac{ne}{2\epsilon_o \bar{V}_s} \right)^{1/2}. \quad (27)$$

We obtain the mean sheath width \bar{s} in terms of mean sheath voltage \bar{V}_s by using the collisionless Child-Langmuir law

$$\bar{s} = \frac{2}{3} \left(\frac{2e}{M} \right)^{1/4} \left(\frac{\epsilon_o}{J_i} \right)^{1/2} \bar{V}_s^{3/4}. \quad (28)$$

The ion current density is $J_i = n_s e v_B$, where n_s is the ion concentration at the presheath-sheath boundary and v_B is the Bohm velocity. Let $V_1 = kT_e/(2e)$ be the presheath voltage drop. Then, $n_s = n \exp(-eV_1/(k_B T_e)) = n \exp(-1/2) = 0.61n$, and $J_i = 0.61ne(kT_e/M)^{1/2}$. This implies

$$\bar{s} = \frac{2}{3} \left(\frac{2e}{kT_e} \right)^{1/4} \left(\frac{\epsilon_o}{0.61ne} \right)^{1/2} \bar{V}_s^{3/4}. \quad (29)$$

And

$$\frac{\omega_{pi}}{\omega_{ion}} = \frac{0.91}{\pi} \left(\frac{2e}{kT_e} \right)^{1/4} \bar{V}_s^{1/4} = \frac{0.91}{\pi} \left(\frac{\bar{V}_s}{V_1} \right)^{1/4}. \quad (30)$$

For typical operating conditions, $V_1 = kT_e/2 = 1$ V, and $\bar{V}_s = 100$ V so that $\omega_{pi}/\omega_{ion} \sim 1$. Thus, it is not surprising that ω_{pi} and ω_{ion} are used interchangeably in the literature. However, strictly speaking, it is ω_{ion} that determines the ion behavior in the sheath and not ω_{pi} , which is the natural frequency of the ion in the bulk plasma.

III. 1d3v Simulation of a Current-Driven RF Sheath

We conducted some particle-in-cell simulations of a current-driven collisionless rf plasma sheath in order to illustrate the resulting ion energy distributions. Figure 3 shows our model for the current-driven sheath. We used our bounded 1d3v particle-in-cell plasma code PDP1.⁴⁴ In the simulation, there were two electrodes connected by an external circuit. The source electrode was grounded, and the target electrode was capacitively coupled to a sinusoidal current source. Electrons and helium ions were emitted from the source electrode at thermal velocities. As electrons and helium ions accumulated between the electrodes, an rf ion sheath developed at the target electrode. After a steady-state was reached, various diagnostics were recorded. We chose a current-driven sheath in order to avoid arbitrarily setting the target potential dc bias.

PDP1 Model of Current-Driven Sheath

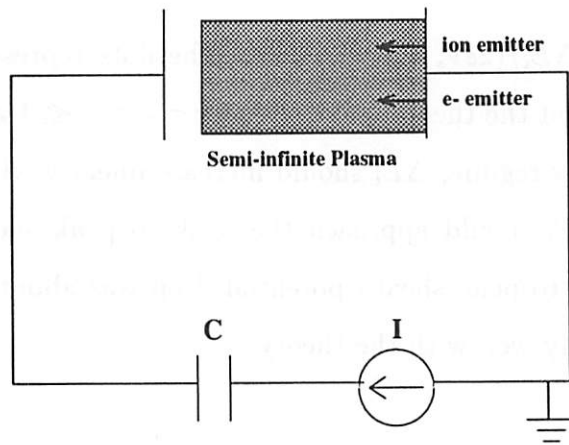


Figure 3:

Figure 4 shows the IEDs for various applied frequencies. In each case, input parameters were chosen so that the ion transit frequency $\omega_{ion}/(2\pi) \approx 13$ MHz. As expected, we see bimodal distributions which become narrower as the frequency increases.

IEDs of He Gas at Various Frequencies(Hz)

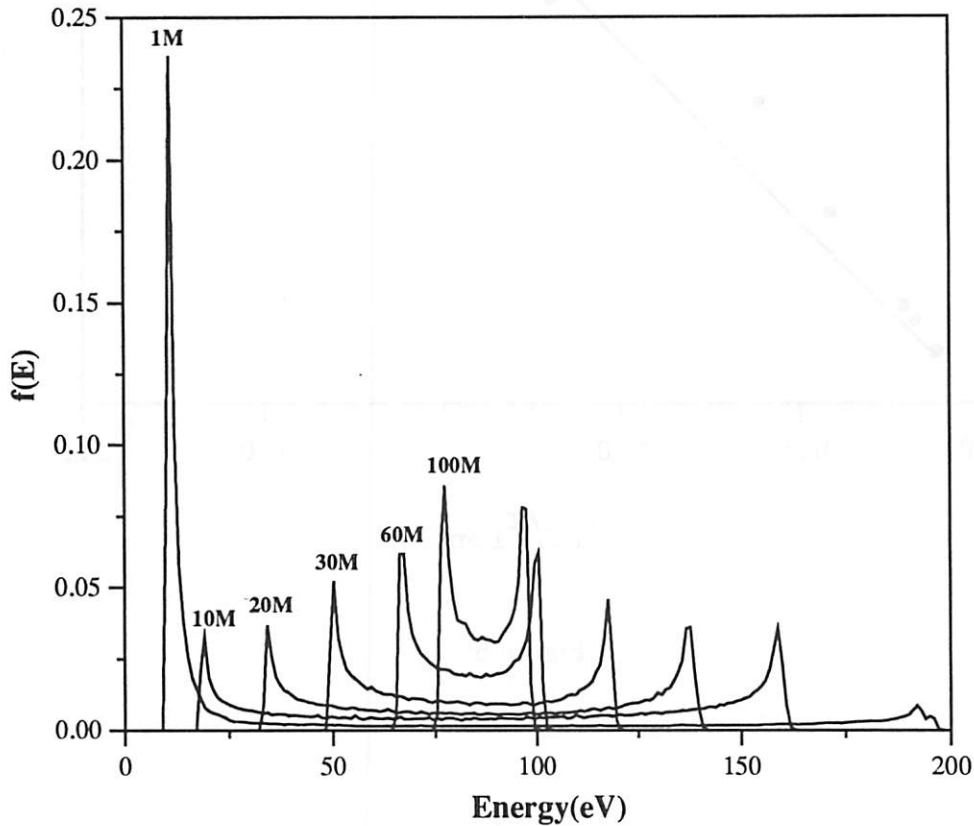


Figure 4:

Figure 5 is a plot of $\Delta E_i / (2e\tilde{V}_s)$ vs. τ_{rf} / τ_{ion} . The dots represent the simulation data while the two lines represent the theoretical curves for $\tau_{rf} / \tau_{ion} \ll 1$ and $\tau_{rf} / \tau_{ion} \gg 1$. Recall that for the high frequency regime, ΔE_i should increase linearly with τ_{rf} / τ_{ion} . And for the low frequency regime, ΔE_i should approach the peak to peak sheath potential drop. In our simulations, the peak to peak sheath potential drop was about 200 V. The simulation appears to agree reasonably well with the theory.

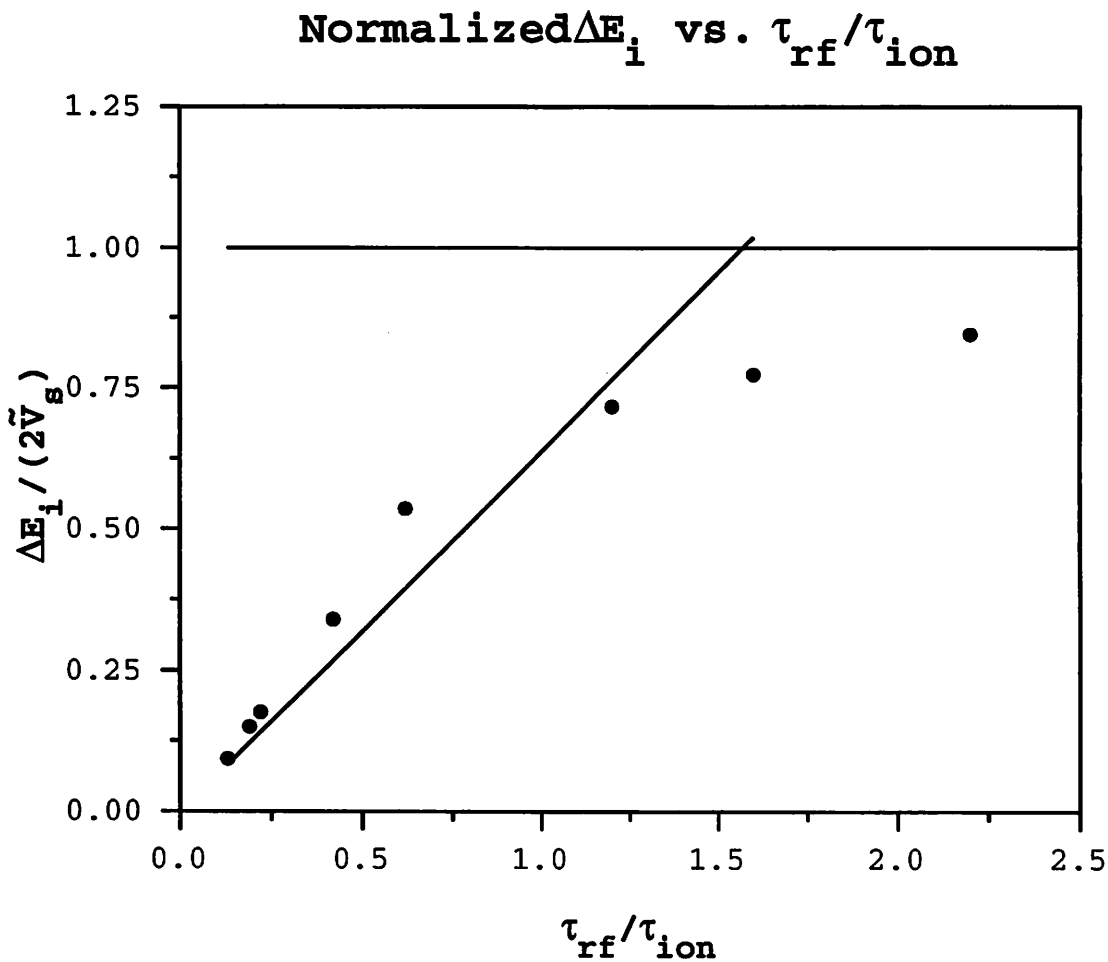


Figure 5:

From equation 3, we also know that for low τ_{rf}/τ_{ion} , ΔE_i is a linear function of \tilde{V}_s , the rf part of the sheath voltage. We conducted a complementary set of simulations in which τ_{rf}/τ_{ion} was held fixed while we varied \tilde{V}_s . Figure 6 depicts the results of these simulations, showing the expected linear relation between ΔE_i and \tilde{V}_s . For this set of simulations, we used CF_3 rather than He ions and kept the frequency of the current source fixed at 13.56 MHz.

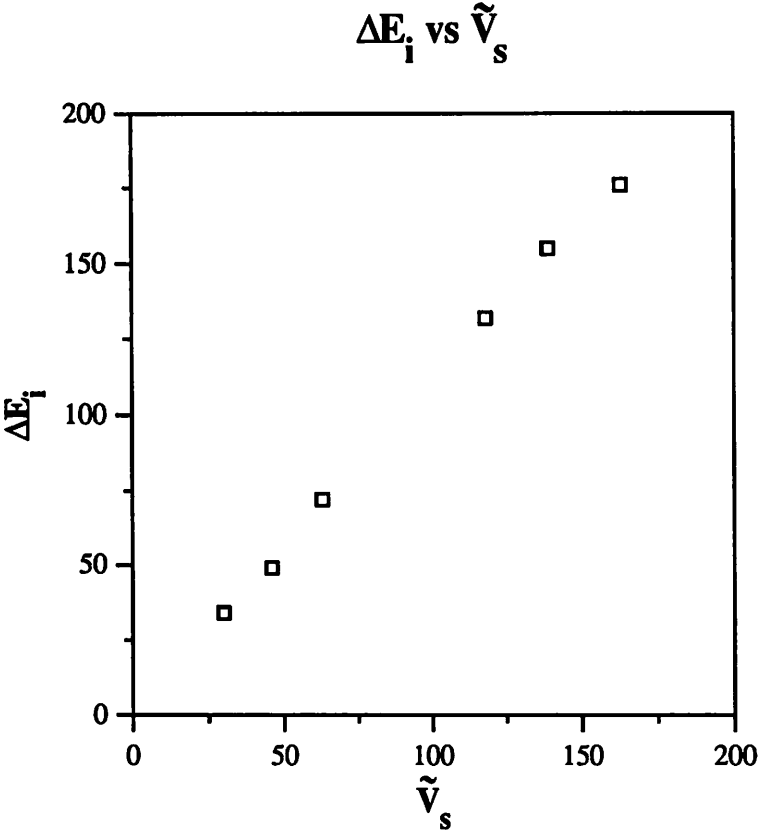


Figure 6:

For low frequencies (i.e., $\tau_{ion}/\tau_{rf} \ll 1$), we expect the sheath voltage to stay at a minimum value for a longer part of the cycle than at a maximum value, resulting in an IED with a dominant low energy peak. Whereas, for high frequencies, (i.e., $\tau_{ion}/\tau_{rf} \gg 1$), we expect the sheath voltage to be nearly sinusoidal, resulting in peaks of more or less equal heights. From Figures 7, we see that the sheath voltage waveforms and the relative dominance of the peaks are as expected. In the high frequency regime (i.e., 100 MHz), the peaks are nearly equal in height while in the low frequency case (i.e., 1 MHz), the low energy peak dominates.

IC-04/12 2.0

IEDs and Sheath voltages for He gas at 1 MHz and 100 MHz

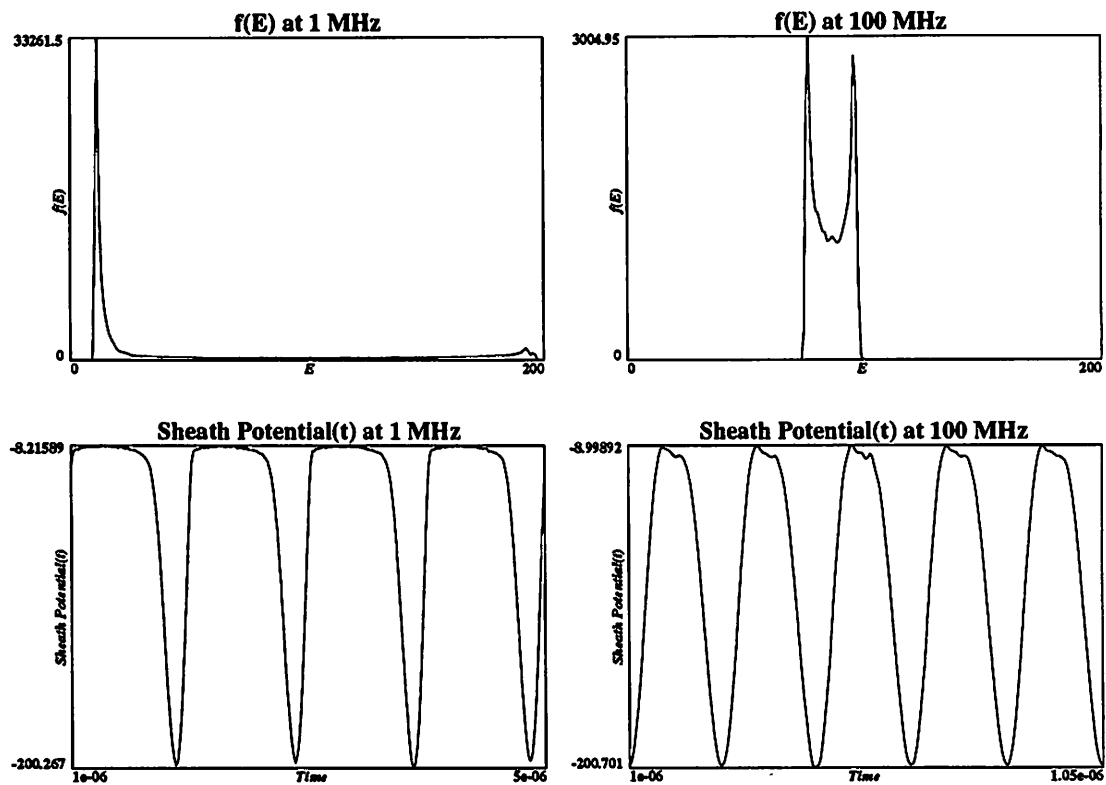


Figure 7:

Also, from Figure 8, we see that for the low frequency regime (i.e., 100 MHz), the conduction current dominates and the sheath is resistive while for the high frequency regime (i.e., 1 MHz), the displacement current dominates and the sheath is capacitive.

Figure 8

**Total, Conduction, and Displacement
Currents at 1 MHz and 100 MHz**

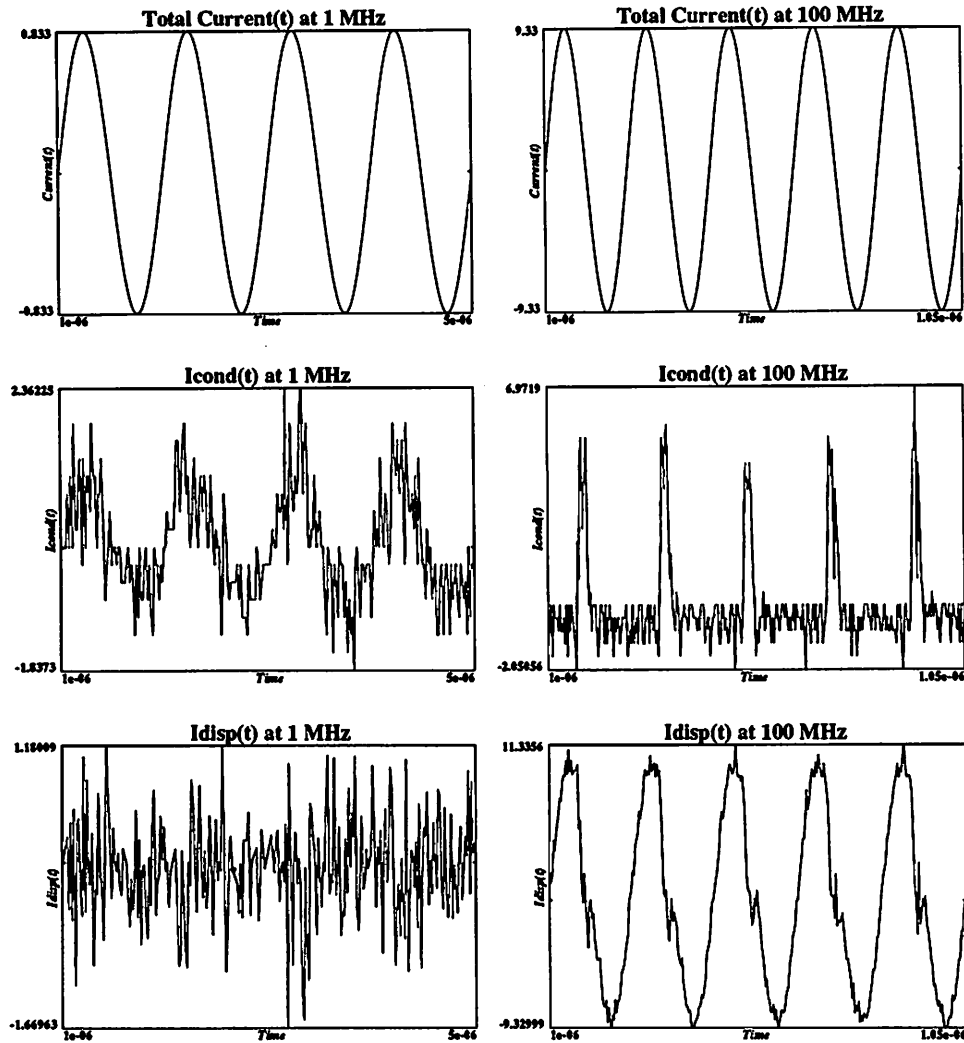


Figure 8:

IV. Conclusion

For collisionless rf plasma sheaths, the ratio τ_{ion}/τ_{rf} determines the nature of the sheath and the shape of the IEDs. For, $\tau_{ion}/\tau_{rf} \ll 1$, the sheath is resistive, and the IED is broad and bimodal with a dominant low energy peak. As we increase τ_{ion}/τ_{rf} , the sheath becomes capacitive, the peaks become more equal in height, and the IED width decreases until at some point the two peaks merge and cannot be resolved.

V. Acknowledgements

The authors gratefully acknowledge support from the Lawrence Livermore National Laboratory under U.S. Department of Energy Contract W-7405-ENG-48, U.S. Department of Energy Contract DE-FG03-90ER54079, and, in Berkeley Office of Naval Research Contract FD-N00014-90-J-1198.

VI. Appendix: Computer Experiment Input File

The following is the PDP1 input deck used for Figures 4,5,7 and 8 to simulate a current-driven collisionless rf sheath. The two species used were *He* ions and electrons. To run simulations at different frequencies, only the f_0 (frequency of current source) and ac (amplitude of current source) parameters were altered. The ac parameter was modified in order to keep the peak to peak sheath voltage the same for each frequency.

The PDP1 input deck used for Figure 6 is similar to this one except that CF_3 ions were used instead of *He* ions, the frequency is kept fixed at 13.56 MHz, and only the parameter ac was changed in order to change the rf sheath voltage.

RF Sheath(IN MKS UNITS)

```

-nsp---nc---nc2p---dt[s]---length[m]--area[m^2]--epsilon_r--B[Tesla]---PSI[D]--
  2   100  1e8  3.90625e-11   0.005   0.016   1.0   0.0   0.0
-rhoback[C/m^3]---backj[Amp/m^2]---dde--extR[Ohm]--extL[H]---extC[F]---q0[C]-
  0.0   0.0   0.0   0.0   0.0   0.0   1.0   0.0
-dcramped--source--dc[V|Amp]--ramp[(V|Amp)/s]---ac[V|Amp]---f0[Hz]--theta0[D]-
  0     i     0.0   0.0   9.33  1e8   0.0
--secondary---e_collisional---i_collisional---reflux---nfft--nsmoothing--ntimestep-
  0     0     0     0     256   0     0
--seec(electrons)---seec(ions)---ion species---Gpressure[Torr]---GTemp[eV]---
  0.0   0.0   1     5e-3   .026

```

SPECIES 1

```

----q[C]-----m[Kg]---j0L[Amp/m^2]---j0R[Amp/m^2]----initn[m^-3]--
  1.602e-19  6.7e-27   0.0   35.2   0.0
--v0L[m/s]---v0R[m/s]---vtL[m/s]---vtR[m/s]----vcL[m/s]---vcR[m/s]-
  0.0   0.0   2.2e3  2.2e3   0.   0.
---vperpt[m/s]---vperp0[m/s]---nbin----Emin[eV]----Emax[ev]---max-np--
  2.2e3   0.0   200   0   200   50000
-For-Mid-Diagnostic---nbin----Emin[eV]---Emax[eV]----XStart--XFinish--
  200   0.0   200   .0025  .003

```

SPECIES 2

```

----q[C]-----m[Kg]---j0L[Amp/m^2]---j0R[Amp/m^2]----initn[m^-3]--
  -1.602e-19  9.11e-31   0.0   9600   0.00
--v0L[m/s]---v0R[m/s]---vtL[m/s]---vtR[m/s]----vcL[m/s]---vcR[m/s]-
  0.0   0.0   6e5   6e5   0.   0.
---vperpt[m/s]---vperp0[m/s]---nbin----Emin[eV]----Emax[ev]---max-np--
  6e5   0.0   200   0   200   50000
-For-Mid-Diagnostic---nbin----Emin[eV]---Emax[eV]----XStart--XFinish--
  200   0.0   200   .0025  .003

```

References

- ¹R. A. Gottscho, C. W. Jurgensen, and D. J. Vitkavage, "Microscopic uniformity in plasma etching," *J. Vac. Sci. Technol. B* **10** 2133 (1992).
- ²E. S. Shaqfeh and C. W. Jurgensen, "Simulation of reactive ion etching pattern transfer," *J. Appl. Phys.* **66**, 4664 (1989).
- ³C. B. Zarowin, "Relation between the RF discharge parameters and plasma etch rates, selectivity, and anisotropy," *J. Vac. Sci. Technol. A* **2**, 1537 (1984).
- ⁴C. Wild and P. Koidl, "Structured ion energy distribution in radio frequency glow-discharge systems," *Appl. Phys. Lett.* **54**, 505 (1989).
- ⁵C. Wild and P. Koidl, "Ion and electron dynamics in the sheath of radio-frequency glow discharges," *J. Appl. Phys.* **69**, 2909 (1990).
- ⁶J. Liu, G. L. Huppert, and H. H. Sawin, "Ion bombardment in rf plasmas," *J. Appl. Phys.* **68**, 3916 (1990).
- ⁷A. Manenschijn and W. J. Goedheer, "Angular ion and neutral energy distribution in a collisional rf sheath," *J. Appl. Phys.* **69**, 2923 (1991).
- ⁸M. Fivaz, S. Brunner, W. Schwarzenbach, A. A. Howling and Ch. Hollenstein, Ecole Polytechnique Fédérale de Lausanne, Preprint: "Reconstruction of the time-averaged sheath potential profile in an argon RF plasma using the ion energy distribution."
- ⁹W. D. Davis and T. A. Vanderslice, "Ion Energies at the Cathode of a Glow Discharge," *Phys. Rev.* **131**, 219 (1963).
- ¹⁰V. Vahedi, M. A. Lieberman, M. V. Alves, J. P. Verboncoeur, and C. K. Birdsall, "A one-dimensional collisional model for plasma-immersion ion implantation," *J. Appl. Phys.* **69**, 2008 (1991).

- ¹¹C. Charles, R. W. Boswell and R. K. Porteous, "Measurement and modeling of ion energy distribution functions in a low pressure argon plasma diffusing from a 13.56 MHz helicon source," *J. Vac. Sci. Technol. A* **10**, 398 (1992).
- ¹²R.A. Gottscho, "Ion transport anisotropy in low pressure, high-density plasmas," *J. Vac. Sci. Technol. B* **11**, 1884 (1993).
- ¹³W.M. Holber and J. Forster, "Ion energetics in electron cyclotron resonance discharges," *J. Vac. Sci. Technol. A* **8**, 3720 (1990).
- ¹⁴J. Hopwood, "Ion bombardment energy distributions in a radio frequency induction plasma," *Appl. Phys. Lett.* **62**, 940 (1993).
- ¹⁵P. Benoit-Cattin, L. C. Bernard, et A. Bordenave-Montesquieu, "Dispersion en énergie des ions produits par une source à excitation de haute fréquence," *Entropie* **18**, 29 (1967).
- ¹⁶P. Benoit-Cattin and L. C. Bernard, "Anomalies of the Energy of Positive Ions Extracted from High-Frequency Ion Sources. A Theoretical Study," *J. Appl. Phys.* **39**, 5723 (1968).
- ¹⁷R.T. Farouki, S. Hamaguchi, and M. Dalvie, "Analysis of a kinematic model for ion transport in rf plasma sheaths," *Phys. Rev. A* **45**, 5913 (1992).
- ¹⁸R. T. C. Tsui, "Calculation of Ion Bombarding Energy and Its Distribution in rf Sputtering," *Phys. Rev.* **168**, 107 (1968).
- ¹⁹A. Metze D. W. Ernie, and H. J. Oskam, "The energy distribution of ions bombarding electrode surfaces in rf plasma reactors," *J. Appl. Phys.* **65**, 993 (1989).
- ²⁰D. Field, D. F. Klemperer, P.W. May, and Y. P. Song, "Ion energy distributions in radio-frequency discharges," *J. Appl. Phys.* **70**, 82 (1991).
- ²¹M. J. Kushner, "Distribution of ion energies incident on electrodes in capacitively coupled rf discharges," *J. Appl. Phys.* **58**, 4024 (1985).
- ²²B. E. Thompson, H. H. Sawin and Donald Fischer, "Monte-Carlo simulation of ion transport through rf glow-discharge sheaths," *J. Appl. Phys.* **63**, 2241 (1988).

- ²³M. S. Barnes, J. C. Forster, and J. H. Keller, "Ion Kinetics in Low-Pressure, Electropositive, RF Glow Discharge Sheaths," *IEEE Trans. on Plasma Sci.* **19**, 240 (1991).
- ²⁴P.W. May, D. Field, and D. F. Klemperer, "Modeling radio-frequency discharges: Effects of collisions upon ion and neutral particle energy distributions," *J. Appl. Phys.* **71**, 3721 (1992).
- ²⁵H. H. Hwang, M. J. Kushner, "Ion energy distributions in radio frequency discharges sustained in gas mixtures obtained using a Monte-Carlo-fluid hybrid model: endothermic processes and ion Holes," *Plasma Sources Sci. Technol.* **3**, 190 (1994).
- ²⁶D. Vender and R. W. Boswell, "Numerical Modeling of Low-Pressure RF Plasmas," *IEEE Trans. on Plasma Sci.* **18**, 725 (1990).
- ²⁷M. Surendra and D. B. Graves, "Particle Simulation of Radio-Frequency Glow Discharges," *IEEE Trans. on Plasma Sci.* **19**, 144 (1991).
- ²⁸J. Erö, "Radiofrequency modulation in the Thoneman ion source," *Nuclear Instruments* **3**, 303 (1958).
- ²⁹Y. Okamoto and H. Tamagawa, "Energy Dispersion of Positive Ions Effused from an RF Plasma," *J. Phys. Soc. Japan*, **29**, 187 (1970).
- ³⁰J. W. Coburn and E. Kay, "Positive-ion bombardment of substrates in rf diode glow discharge sputtering," *J. Appl. Phys.* **43**, 4965 (1972).
- ³¹K. Kohler, D. E. Horne, and J. W. Coburn, "Frequency dependence of ion bombardment of grounded surfaces in rf argon glow discharges in a planar system," *J. Appl. Phys.* **58**, 3350 (1985).
- ³²A. D. Kuypers and H. J. Hopman, *J. Appl. Phys.*, "Ion energy measurement at the powered electrode in an rf discharge," **63**, 1894 (1988).
- ³³A. Manenschijn, G. C. A. M. Janssen, E. van der Drift and S. Radelaar, "Measurement of ion impact energy and ion flux at the rf electrode of a parallel plate reactive ion etcher," *J. Appl. Phys.* **69** 1253 (1991).

- ³⁴W. M. Greene, M.A. Hartney, W.G. Oldham, and D. W. Hess, "Ion transit through capacitively coupled Ar sheaths: Ion current and energy distribution," *J. Appl. Phys.* **63**, 1367 (1988).
- ³⁵J. Janes and C. Huth, "Energy-resolved angular distributions of O^+ ions at the radio-frequency-powered electrode in reactive ion etching," *J. Vac. Sci. Technol. A* **10**, 3086 (1992).
- ³⁶J. Janes and C. Huth, "Energy-resolved angular distributions of O^+ ions at the radio-frequency-powered electrode in reactive ion etching," *J. Vac. Sci. Technol. A* **10**, 3522 (1992).
- ³⁷J. Janes, "Mass-selected ion angular impact energy distributions at the powered electrode in CF_4 reactive-ion etching," *J. Appl. Phys.* **74**, 659 (1993).
- ³⁸J. K. Olthoff, R.J. Van Brunt and S. B. Radovanov, "Ion kinetic-energy distributions in argon rf glow discharges," *J. Appl. Phys.* **72**, 4566 (1992).
- ³⁹J. K. Olthoff, J. Van Brunt, S. B. Radovanov, J. A. Rees and R. Surowiec, "Kinetic-energy distributions of ions sampled from argon plasmas in a parallel-plate, radio-frequency reference cell," *J. Appl. Phys.* **75**, 115 (1994).
- ⁴⁰R. J. M. M. Snijkers, M. J. M. van Sambeek, B. M. W. Kroesen and F. J. de Hoog, "Mass-resolved ion energy measurements at the grounded electrode of an argon rf plasma," *Appl. Phys. Lett.* **63**, 308 (1993).
- ⁴¹U. Flender and K. Wiesemann, "Ion distribution functions behind an RF sheath," *J. Phys. D: Appl. Phys.* **27**, 509 (1994).
- ⁴²A. Metze, D. W. Ernie, and H.J. Oskam, "Application of the physics of plasma sheaths to the modeling of rf plasma reactors," *J. Appl. Phys.* **60**, 3081 (1986).
- ⁴³M. A. Lieberman, "Analytical solution for capacitive RF sheath," *IEEE Trans. on Plasma Sci.* **16**, 4375 (1988).

⁴⁴C. K. Birdsall, "Particle-in-cell charged-particle simulations, plus Monte Carlo collisions with neutral atoms, PIC-MCC," *IEEE Trans. on Plasma Sci.* **19**, 65 (1991).